Chemical Engineering Journal 348 (2018) 929–939

Contents lists available at ScienceDirect

Chemical Engineering Journal

journal homepage: www.elsevier.com/locate/cej

One-step production of biodiesel from *Jatropha* oils with high acid value at low temperature by magnetic acid-base amphoteric nanoparticles

Yi-Tong Wang[a,d], Zhen Fang[b,*], Xing-Xia Yang[a,d], Ya-Ting Yang[a], Jia Luo[a], Kun Xu[c], Gui-Rong Bao[c]

[a] *Biomass Group, Key Laboratory of Tropical Plant Resources and Sustainable Use, Xishuangbanna Tropical Botanical Garden, Chinese Academy of Sciences, 88 Xuefu Road, Kunming, Yunnan Province, 650223, China*
[b] *Biomass Group, College of Engineering, Nanjing Agricultural University, 40 Dianjiangtai Road, Nanjing, Jiangsu 210031, China*
[c] *Faculty of Metallurgical and Energy Engineering, Kunming University of Science and Technology, Kunming, Yunnan Province, 650093, China*
[d] *University of Chinese Academy of Sciences, 19A Yuquan Road, Beijing 100049, China*

HIGHLIGHTS

- Biodiesel production was catalyzed with magnetic acid-base amphoteric nanoparticles (< 46 nm).
- $Zn_8@Fe\text{-}C_{400}$ nanoparticles presented good activity, stability and reusability.
- Strong magnetism for $Zn_8@Fe\text{-}C_{400}$ nanoparticles benefitted the continuous biodiesel production.
- *Jatropha* biodiesel yield of 100.0% was achieved for $Zn_8@Fe\text{-}C_{400}$ without saponification.
- $Zn_8@Fe\text{-}C_{400}$ was cycled for at least 10 times with biodiesel yield of > 94.3%.

GRAPHICAL ABSTRACT

Alkaline oxides concerted with acidic -COOFe structure, for the one-pot esterification and transesterification of high AV *Jatropha* oils without saponification. $Zn_8@Fe\text{-}C_{400}$ nanoparticles achieved nearly 100% *Jatropha* biodiesel yield at 160 °C within 4h, and was used for at least 10 cycles with biodiesel yield of > 94.3% at acid value of 6.3 mg KOH/g.

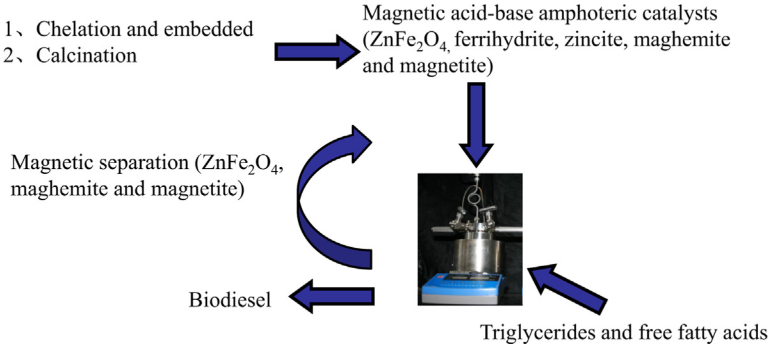

ARTICLE INFO

Keywords:
Acid-base amphoterism
High acid value
Jatropha biodiesel
Magnetic nanoparticles
One-step production

ABSTRACT

Biodiesel production from *Jatropha* oils with high acid value at low temperature was catalyzed with synthesized novel magnetic acid-base amphoteric nanoparticles (< 46 nm). Alkaline oxides ($ZnFe_2O_4$, ferrihydrite, zincite, maghemite and magnetite) concerted with acidic -COOFe structure, benefited the one-pot esterification and transesterification of *Jatropha* oils with high acid value to produce biodiesel without additional pretreatment. The strong magnetism of catalyst helped catalyst separation for recycle in continuous biodiesel production. *Jatropha* biodiesel yield of 100% at 160 °C within 4 h, with methanol/oil molar ratio of 40/1 and catalyst dosage of 7 wt% was achieved, while the catalyst can be cycled for at least 10 times with biodiesel yield > 94.3% at acid value of 6.3 mg KOH/g. No obvious saponification was observed during the reactions and storage.

---

* Corresponding author.
E-mail address: zhenfang@njau.edu.cn (Z. Fang).
URL: http://biomass-group.njau.edu.cn/ (Z. Fang).

https://doi.org/10.1016/j.cej.2018.05.039
Received 12 December 2017; Received in revised form 20 April 2018; Accepted 7 May 2018
Available online 08 May 2018

1. Introduction

Increasing trend of modernization and industrialization leads to rapid depletion of the fossil fuels [1,2] and long-term environmental pollution [3,4]. While renewable bio-based oils [5] taking the place of mineral ones seem to be inevitable for energy use in the near future due to sustainable development and eco-friendly. Biodiesel (fatty acid methyl esters; FAMEs) [2,6], one typical and ideal alternative to diesel, can be produced from edible oils [7,8] and non-edible oils [9–12] by esterification and transesterification process using homogeneous or heterogeneous catalysts. In recent decades, it acquires more and more attentions based on its good characteristics [13]. These researches report that the production and use of biodiesel can reduce emissions of 78% CO_2, 79% waste water and 96% hazardous wastes as compared with fossil diesel [14]. Under the same enzyme action conditions, 80.4–91.2% biodiesel can be biodegraded as compared with only 24.5%-24.5% for fossil diesel after 30 days [15]. In addition, biodiesel can be used in diesel engines after several blends without or with minimal engine modifications [2,16], and the usage of mixed biodiesel and diesel can improve fuel qualities [17]. At present, more than 350 oil-bearing crops are identified as potential raw materials for biodiesel production [18]. Cheaper non-edible oils [16] are more welcomed as raw materials because of the deficit of edible oils in many developing countries and their use reduces the biodiesel production costs [19]. However, high free fatty acids (FFAs) content produces serious trouble for the utilization of most non-edible oils [20]. Saponification easily happens during the catalytic reactions of non-edible oils with base catalysts [21], which results in great difficulty for the continuous biodiesel production and seriously corrupted quality of obtained biodiesel. Hence, additional deacidification is required to convert FFAs to methyl esters before base-catalyzed transesterification, using acid catalysts [22–24]. This traditional two-step method requires complex separation and purification processes with a large amount of waste water produced, and decreases the chemical and environmental economics of fuel production process. Brønsted acids can catalyze both esterification and transesterification in one step, however, it requires much severer conditions (e.g., 220 °C) [24]. The active acid sites are unstable at high temperatures, and are inclined to leach during reactions. Boey et al. propose a new method to synthesize Lewis solid acid by chelation with sodium alginate and Fe^{3+} to esterify FFAs to biodiesel, but it only catalyzes esterification reaction [25,26]. While biodiesel mainly comes from the transesterification of triglycerides. Our previous work improves the above synthesis method to create bifunctional magnetic solid acid with both Lewis and Brønsted acid sites that can catalyze the simultaneous esterification and transesterification reactions of high acid value (AV) oils to biodiesel [27]. When the content of FFAs in crude oil is greater than triglycerides, bifunctional magnetic solid acid is a very good choice as the catalyst. However, the main components of plant oils are triglycerides, in this situation, it shows poor catalytic activity for transesterification because base-catalyzed transesterification is 4000 times faster than acid catalysis [28]. Therefore, novel concept should be proposed to solve this problem for the catalytic transformation of non-edible oils with high AV, such as *Jatropha* oil with triglycerides as main components. Both acidic and basic sites with considerable magnetism can be introduced in catalyst for the simultaneous esterification and transesterification for biodiesel production without observable saponification. One-step biodiesel production from oils with high AV (e.g., *Jatropha* oil) is proceeding by basic sites catalyze transesterifying triglycerides while acidic sites are for esterifying FFAs and avoiding the contact of FFAs on basic groups for soap formation, magnetic core helping magnetic separation (Scheme 1). At present, few studies are reported for this proposed scheme. Hence, new catalyst synthesis methods should be developed to balance its acidity, basicity and magnetism.

In this work, biodiesel production from *Jatropha* oils with high AV at low temperature was catalyzed with a series of heterogeneous magnetic acid-base particles synthesized. These catalysts had following specialities: (i) Both strong Lewis acidity and strong basicity, with excellent catalytic activity during the reactions; (ii) Without observable saponification; and (iii) Strong magnetism for their easy recovery and benefited catalyst recycles for biodiesel production. Various techniques were also used to characterize catalysts.

2. Experimental

2.1. Materials

Analytical reagents MgO (≥98.0%), Al_2O_3 (100–200 mesh), ZnO (≥99.0%), Na_2SiO_3 (SiO_2 44–47%) and $Fe_2(SO_4)_3$ (≥99.7%, Fe content of 21–23%) were purchased from Aladdin (Shanghai). Dehydrated methanol (≥99.5%) and dichloromethane (≥99.0%) were from Xilong Chemical Factory Co., Ltd. (Shantou, Guangdong). Sodium carboxymethylcellulose (CMC) with viscosity of 300–800 mPa·s was bought from Sinopharm Chemical Reagent Co., Ltd. (Shanghai). Deionized water was obtained by a water purification system (electrical conductivity of 18.2 MΩ·cm, Milli-Q Academic, Merck Millipore, Darmstadt, Germany). Seven kinds of methyl esters [palmitate ($C_{16:\ 0}$), palmitoleate ($C_{16:\ 1}$), heptadecanoic($C_{17:\ 0}$), stearate ($C_{18:\ 0}$), oleate ($C_{18:\ 1}$), linoleate ($C_{18:\ 2}$) and linolenate ($C_{18:\ 3}$)](≥99.0%) were purchased from Sigma (Shanghai). *Jatropha* oils with AV of 6.3, 12.8 and 17.3 mg KOH/g, and molecular weights of 862.2, 858.7 and 860.0 g/mol were obtained from Yunnan Shenyu New Energy Co., Ltd and Xishuangbanna Tropical Botanical Garden (Menglun, Yunnan), respectively.

2.2. Catalyst preparation and characterization

At room temperature, 200 mL CMC solution with concentration of about 20 g/L was fully mixed with 0.5–8.0 g solid basic particles (MgO, Al_2O_3, ZnO and Na_2SiO_3). The mixed CMC solution was added dropwise in 200 mL, 1.0 mol/L $Fe_2(SO_4)_3$ solution under mechanical stirring, and chelated for 3 h to yield precipitate [25,26] (COOFe-CMC chelate as Lewis acid covered basic particles inside). The precipitate was filtered, washed with distilled water until *pH* reaching nearly 7 and then dried at 105 °C (WFO-710, EYELA, Tokyo Rikakikai Co., Ltd.) overnight. Dry solid residue was calcined at 400, 500 or 600 °C for 2 h (excluding heating and cooling time) under N_2 flushing (flow rate of 400 mL/min) in a tubular furnace (SGL-1100, Shanghai Daheng Optics and Fine Mechanics Co., Ltd.), with heating rate of 1 °C/min (COOFe-CMC was partially reduced to Fe_3O_4, alkaline oxide was activated and new metal oxide was produced, such as $ZnFe_2O_4$ for $Zn_8@Fe\text{-}C_{400}$). The calcined catalysts were grounded to particles with size of < 75 μm, and named as $Mg/Al/Zn/Na_n@Fe\text{-}C_T$, while n was the weight of embedded basic particles (e.g., ZnO), and T was calcination temperature. Pure ZnO particles were also calcined at 400 °C for 2 h, grounded to fine particles with size of < 75 μm for control experiments.

The fresh and recovered $Zn_8@Fe\text{-}C_{400}$ catalysts after 5 cycles were characterized by X-ray diffraction (XRD, Rigaku Rotaflex RAD-C, Tokyo) using CuKα radiation (40 kv and 200 mA). The crystalline size of solid catalysts was calculated based on Scherer equation [29] [$Dc = K\lambda/(\beta\cos\theta)$, (Dc, average particle size; K, Scherer constant, 0.89; λ, X-ray wavelength of CuKα radiation, 0.1541 nm; β, full-width at half-maximum; θ, diffraction angle)]. The surface acidity and basicity of fresh and recovered catalysts were analyzed by CO_2/NH_3-temperature programmed desorption (CO_2/NH_3-TPD; Chemisorption analyzer, Quantachrome Instruments, Boynton Beach, FL). Catalyst (50 mg) was degassed at 100 °C for 60 min to remove physically adsorbed water, and then absorbed CO_2/NH_3 (10% CO_2/NH_3 and 90% He) at 50 °C for 60 min. The absorbed catalyst was heated to 400 °C under pure He for desorption (with heating rate of 5 °C/min). The background curve was obtained by catalyst adsorption under pure He instead of CO_2/NH_3 flow. The TPD results listed in the table were values after removing the

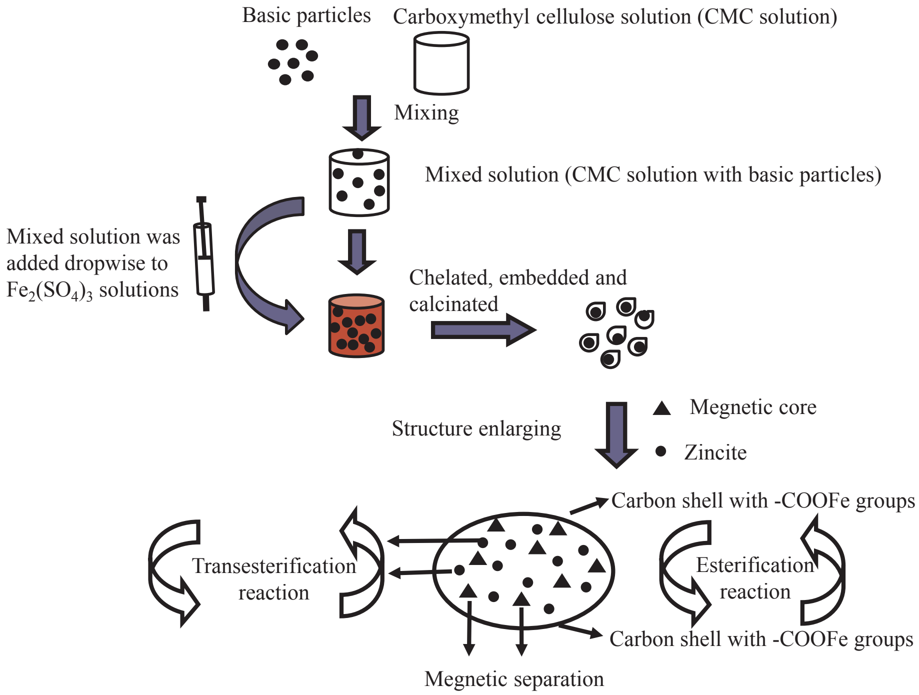

Scheme 1. Workflow of catalyst preparation and application.

background effect. The morphology and EDX maps on the surface of catalysts were examined with scanning electronic microscope-X-ray energy dispersive analysis (SEM-EDX; SU8020, Hitachi, Japan) and transmission electron microscope (TEM, JEM-1200EX, JEOL, Tokyo). Their element contents on the surface were detected by EDX (Quanta 200, FEI, Hillsboro, OR). Thermogravimetric analysis (TG) of fresh and recovered $Zn_8@Fe-C_{400}$ catalysts were conducted on a simultaneous thermal analyzer (STA449F3, NETZSCH-Gerätebau GmbH, Selb, Germany) with temperature ranging from room temperature to 1000 °C (heating rate of 5 °C/min) in N_2. The magnetism of catalysts was detemined by a vibrating sample magnetometer (VSM; lakeshore7407, Lake Shore Cryotronics, Inc., Westerville, OH). Metal ion contents in catalysts were detected by inductively coupled plasma-optical emission spectrometer (ICP-OES; Optima 5300, PerkinElmer Inc, Waltham, MA) after catalyst dissolved in acid solution. Their BET surface area, pore volume and pore size were determined by Bruner-Emmett-Teller (BET) method (Tristar II 3020, Micromeritics Instrument Co., Ltd., Northcross, GA) with N_2 adsorption. Fourier transform-infrared spectra (FT-IR) of catalysts were obtained on Nicolet *is*10 spectrometer (Thermo Fisher Scientific Co. Ltd., Waltham, MA) over the wavenumber ranging from 3800 to 400 cm^{-1} with a resolution of 4 cm^{-1}, using standard KBr disc method. The C contents in fresh and recovered $Zn_8@Fe-C_{400}$ catalysts were measured by an element analyzer (Vario EL III CHONS, Elementar Analysensysteme GmbH, Hanau, Germany).

2.3. One-step production of biodiesel from Jatropha oils with high AV

Crude *Jatropha* oils (4.3 g), dehydrated methanol (6.4 g) and catalyst (0.3 g) were transferred into a 50 mL micro high-pressure autoclave (YZPR-50, Yanzheng Shanghai Experimental Instrument Co., Ltd.) with Teflon lining. The dead volume of reactor was about 9.5 mL. Similar to previous work [11], the reaction conditions for biodiesel production were temperature of 160 °C, time of 4 h (heating time of 25 min was excluded), methanol/oil molar ratio of 40/1, catalyst of 7 wt%, magnetic stirring of 750 rpm and initial pressure of 2 MPa N_2. The maximum pressure during reaction was 4.5 MPa, higher than the saturated vapor pressure (1.75 MPa, calculated according to Perry's Chemical Engineers' Handbook) [30] of methanol at 160 °C. All experiments were repeated twice, and biodiesel yields were average of the individual two runs with standard deviation (σ) of 0.0–2.1%.

Recovery rate of catalyst was defined as:

$$\text{Recovery rate(wt\%)} = (\text{weight of recovered catalyst}) / (\text{weight of fresh catalyst}) \times 100\% \quad (1)$$

After reaction, solid catalysts were separated from liquid products by a NeFeB magnet. The recovered catalysts were washed with pure ethanol and dried for next runs. Crude biodiesel at lower liquid layer was removed to a 50 mL tube, filtered (pore size of 0.22 μm), and dried at 55 °C overnight to remove methanol. Filtered and dried biodiesel was analyzed by gas chromatography (GC; GC-2014, Shimadzu, Kyoto) with a capillary column of Rtx-Wax (30 m × Ø0.25 mm × 0.25 μm) under analytical conditions: injector temperature of 260 °C, column temperature of 220 °C, detector temperature of 280 °C, carrier gas of He (flow rate of 1 mL/min) and split ratio of 40/1. Biodiesel yield was calculated as the total yield of FAMEs in products [Heptadecanoic acid methyl ester (HAME) was used as internal standard]:

$$\text{Weight of FAMEs in product samples} = (\text{Weight of HAME} \times \text{Chromatographic peak area of FAMEs}) / (\text{Chromatographic peak area of HAME} \times \text{Relative response factors for FAMEs}) \quad (2)$$

$$\text{Biodiesel yield(wt\%)} = \sum \text{Weight of FAMEs in products} / \text{Weight of dried crude biodiesel} \times 100\% \quad (3)$$

Chromatographic peaks for palmitate ($C_{16:\,0}$), palmitoleate ($C_{16:\,1}$), stearate ($C_{18:\,0}$), oleate ($C_{18:\,1}$), linoleate ($C_{18:\,2}$) and linolenate ($C_{18:\,3}$) methyl esters were calibrated in previous work [27,31] with relative response factors of (1.01, 1.02, 1.08, 1.04, 1.02 and 0.93), respectively.

3. Results and discussion

Biodiesel production from *Jatropha* oils with high AV at low temperature was catalyzed with the synthesized magnetic acid-base

Table 1

Jatropha biodiesel yield catalyzed by Na$_n$@Fe-C$_T$ catalysts.

Catalysts	Alkaline component	Calcination temperature (°C)	Biodiesel yield (wt%)[a]	Saponification after reactions	Magnetic separation
Na$_{0.5}$@Fe-C$_{400}$	Na$_2$SiO$_3$, 0.5 g	400	46.4 ± 0.0	Yes	> 90%
Na$_{0.5}$@Fe-C$_{500}$	Na$_2$SiO$_3$, 0.5 g	500	50.0 ± 0.1	Yes	> 90%
Na$_{0.5}$@Fe-C$_{600}$	Na$_2$SiO$_3$, 0.5 g	600	15.0 ± 0.0	Yes	> 90%
Na$_8$@Fe-C$_{400}$	Na$_2$SiO$_3$, 8.0 g	400	84.6 ± 1.1	Yes	> 90%
Na$_8$@Fe-C$_{500}$	Na$_2$SiO$_3$, 8.0 g	500	91.3 ± 1.6	Yes	> 90%
Na$_8$@Fe-C$_{600}$	Na$_2$SiO$_3$, 8.0 g	600	99.4 ± 0.1	Yes	> 90%

[a] Reaction conditions: 160 °C, 4.5 MPa, 4 h, catalyst dosage of 7 wt%, methanol/oil molar ratio of 40/1 with 4.3 g *Jatropha* oil (AV of 6.3 mg KOH/g), magnetic stirring of 750 rpm and initial N$_2$ pressure of 2 MPa.

Table 2

Jatropha biodiesel yield catalyzed by Al$_n$@Fe-C$_T$ catalysts.

Catalysts	Alkaline component	Calcination temperature (°C)	Biodiesel yield (wt%)[a]	Saponification after reactions	Magnetic separation
Al$_{0.5}$@Fe-C$_{400}$	Al$_2$O$_3$, 0.5 g	400	15.3 ± 0.3	No	> 90%
Al$_{0.5}$@Fe-C$_{500}$	Al$_2$O$_3$, 0.5 g	500	15.2 ± 0.0	No	> 90%
Al$_{0.5}$@Fe-C$_{600}$	Al$_2$O$_3$, 0.5 g	600	19.9 ± 1.1	No	> 90%
Al$_2$@Fe-C$_{400}$	Al$_2$O$_3$, 2.0 g	400	22.2 ± 0.3	No	> 90%
Al$_2$@Fe-C$_{500}$	Al$_2$O$_3$, 2.0 g	500	20.5 ± 0.1	No	> 90%
Al$_2$@Fe-C$_{600}$	Al$_2$O$_3$, 2.0 g	600	23.0 ± 1.1	No	> 90%
Al$_4$@Fe-C$_{400}$	Al$_2$O$_3$, 4.0 g	400	17.4 ± 1.3	No	> 90%
Al$_4$@Fe-C$_{500}$	Al$_2$O$_3$, 4.0 g	500	18.1 ± 1.3	No	> 90%
Al$_4$@Fe-C$_{600}$	Al$_2$O$_3$, 4.0 g	600	53.3 ± 0.2	No	> 90%
Al$_8$@Fe-C$_{400}$	Al$_2$O$_3$, 8.0 g	400	20.7 ± 0.2	No	< 40%
Al$_8$@Fe-C$_{500}$	Al$_2$O$_3$, 8.0 g	500	- [c]	No	< 40%
Al$_8$@Fe-C$_{600}$	Al$_2$O$_3$, 8.0 g	600	64.9 ± 0.7	No	< 40%

[a] Reaction conditions: 160 °C, 4.5 MPa, 4 h, catalyst dosage of 7 wt%, methanol/oil molar ratio of 40/1 with 4.3 g *Jatropha* oil (AV of 6.3 mg KOH/g), magnetic stirring of 750 rpm and initial N$_2$ pressure of 2 MPa.

Table 3

Jatropha biodiesel yield catalyzed by Mg$_n$@Fe-C$_T$ catalysts.

Catalysts	Alkaline component	Calcination temperature (°C)	Biodiesel yield (wt%)[a]	Saponification after reactions	Magnetic separation
Mg$_2$@Fe-C$_{400}$	MgO, 2.0 g	400	96.8 ± 0.8	No	> 90%
Mg$_2$@Fe-C$_{500}$	MgO, 2.0 g	500	96.6 ± 1.1	No	> 90%
Mg$_2$@Fe-C$_{600}$	MgO, 2.0 g	600	94.1 ± 0.0	No	> 90%
Mg$_4$@Fe-C$_{400}$	MgO, 4.0 g	400	93.5 ± 0.1	No	> 90%
Mg$_4$@Fe-C$_{500}$	MgO, 4.0 g	500	92.0 ± 0.1	No	> 90%
Mg$_4$@Fe-C$_{600}$	MgO, 4.0 g	600	90.7 ± 0.7	No	> 90%
Mg$_8$@Fe-C$_{400}$	MgO, 8.0 g	400	90.6 ± 0.5	No	> 90%
Mg$_8$@Fe-C$_{500}$	MgO, 8.0 g	500	96.3 ± 0.1	No	> 90%
Mg$_8$@Fe-C$_{600}$	MgO, 8.0 g	600	99.0 ± 0.8	No	> 90%

[a] Reaction conditions: 160 °C, 4.5 MPa, 4 h, catalyst dosage of 7 wt%, methanol/oil molar ratio of 40/1 with 4.3 g *Jatropha* oil (AV of 6.3 mg KOH/g), magnetic stirring of 750 rpm and initial N$_2$ pressure of 2 MPa.

Table 4

Jatropha biodiesel yield catalyzed by a series of Zn$_n$@Fe-C$_T$ catalysts.

Catalysts	Alkaline component	Calcination temperature (°C)	Biodiesel yield (wt%)[a]	Saponification after reactions	Magnetic separation
Zn$_{0.5}$@Fe-C$_{400}$	ZnO, 0.5 g	400	46.7 ± 0.1	No	> 90%
Zn$_{0.5}$@Fe-C$_{500}$	ZnO, 0.5 g	500	43.4 ± 0.2	No	> 90%
Zn$_{0.5}$@Fe-C$_{600}$	ZnO, 0.5 g	600	41.1 ± 1.1	No	> 90%
Zn$_2$@Fe-C$_{400}$	ZnO, 2.0 g	400	92.9 ± 0.1	No	> 90%
Zn$_2$@Fe-C$_{500}$	ZnO, 2.0 g	500	58.4 ± 0.0	No	> 90%
Zn$_2$@Fe-C$_{600}$	ZnO, 2.0 g	600	53.6 ± 0.1	No	> 90%
Zn$_4$@Fe-C$_{400}$	ZnO, 4.0 g	400	93.4 ± 0.7	No	> 90%
Zn$_4$@Fe-C$_{500}$	ZnO, 4.0 g	500	91.4 ± 0.1	No	> 90%
Zn$_4$@Fe-C$_{600}$	ZnO, 4.0 g	600	78.7 ± 0.1	No	> 90%
Zn$_8$@Fe-C$_{400}$	ZnO, 8.0 g	400	100.0 ± 0.0	No	> 90%
Zn$_8$@Fe-C$_{500}$	ZnO, 8.0 g	500	94.0 ± 1.6	No	> 90%
Zn$_8$@Fe-C$_{600}$	ZnO, 8.0 g	600	89.1 ± 0.4	No	> 90%

[a] Reaction conditions: 160 °C, 4.5 MPa, 4 h, catalyst dosage of 7 wt%, methanol/oil molar ratio of 40/1 with 4.3 g *Jatropha* oil (AV of 6.3 mg KOH/g), magnetic stirring of 750 rpm and initial N$_2$ pressure of 2 MPa.

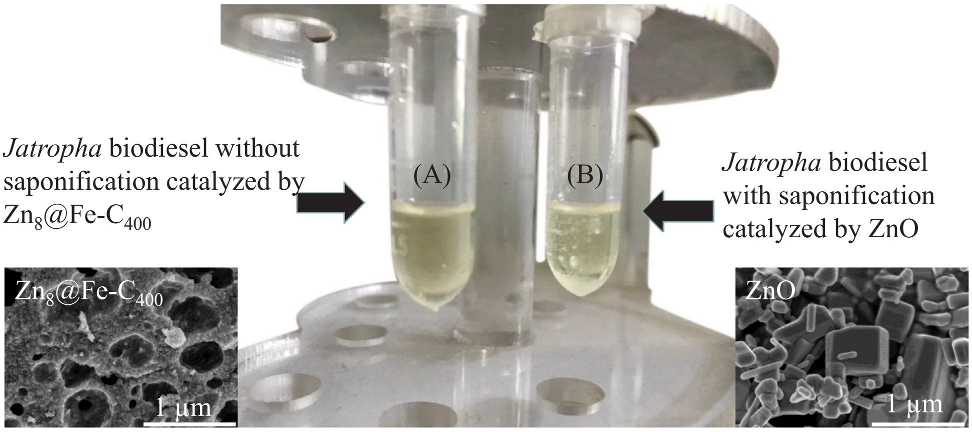

Fig. 1. *Jatropha* biodiesel after half year storage at room temperature catalyzed by (A) $Zn_8@Fe\text{-}C_{400}$ and (B) ZnO catalysts.

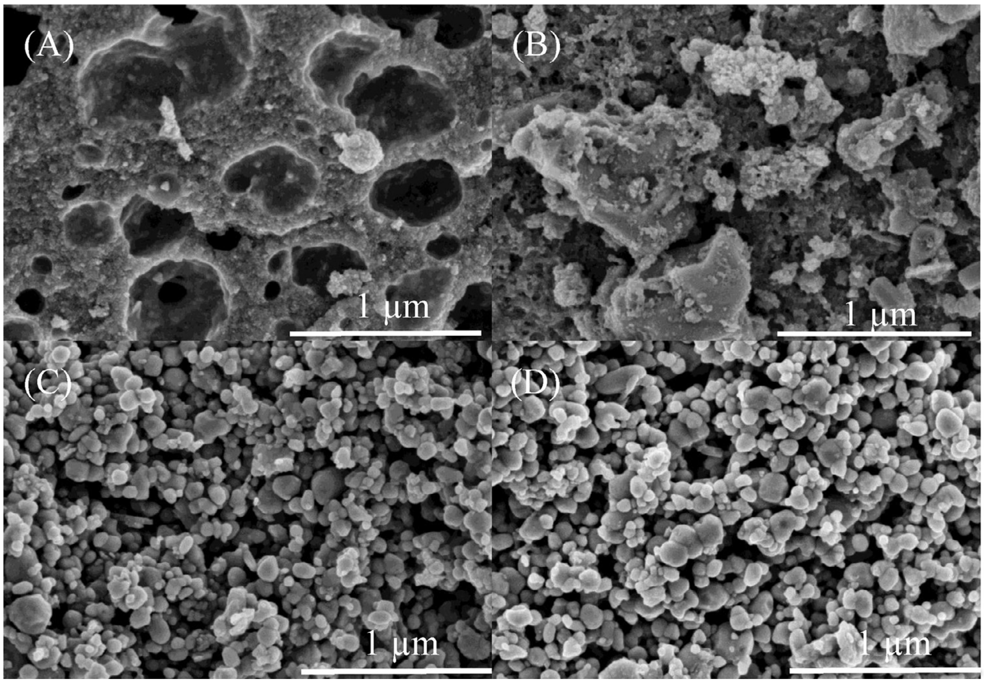

Fig. 2. SEM images of (A) fresh $Zn_8@Fe\text{-}C_{400}$, (B) recovered $Zn_8@Fe\text{-}C_{400}$ catalyst after 5 cycles, (C) fresh $Mg_8@Fe\text{-}C_{600}$ and (D) recovered $Mg_8@Fe\text{-}C_{600}$ catalyst after 5 cycles.

amphoteric particles to screen the most suitable catalyst under the given conditions (160 °C, 4.5 MPa, 40/1 methanol/oil molar ratio, 7 wt % catalyst and 4 h reaction time), and results were listed in Tables 1–4. The saponification conditions of *Jatropha* biodiesel after half year storage at room temperature catalyzed by $Zn_8@Fe\text{-}C_{400}$ and ZnO catalysts were showed in Fig. 1. The morphology (SEM and TEM), EDX maps, thermal stability (TG), magnetic coercivity (VSM), XRD patterns and FT-IR spectra of catalysts were given in Figs. 2–8. Their acidity, basicity, BET surface area, pore volume, pore size, crystalline sizes and elemental compositions were summarized in Tables 5–8.

3.1. One-step production of biodiesel over magnetic amphoteric catalysts

Crude *Jatropha* oil with AV of 6.3 mg KOH/g was selected as crude oil for one-step production of biodiesel. Synergistic catalytic processes were conducted by acidic sites esterifing FFAs and basic sites transesterifing triglycerides. Reaction paths including catalysts synthesis steps, their simplified structures and catalytic processes were proposed in Scheme 1. The introduction of appropriate acid and base sites was important to improve the catalyst activity for one-step production of biodiesel.

3.1.1. Production of biodiesel over magnetic Na-based amphoteric catalysts

Na-based amphoteric catalysts were prepared using Na_2SiO_3 as the basic group and -COOFe as the acidic group. The catalysts were prepared simply through two steps: (i) embedding of Na_2SiO_3 by chelation with Fe^{3+} and CMC solution; and (ii) calcination. The first step packed Na_2SiO_3 in the capsule ball by the chelation of Fe^{3+} with CMC solution to produce both acidic and basic particles, while dried capsule ball was calcined in a tube furnace to create active acidic and basic sites. The calcination simultaneously reduced Fe^{3+} to Fe_3O_4 for magnetizing the catalyst and activated Na_2SiO_3. Synthesized $Na_n@Fe\text{-}C_T$ catalyst showed good activity for biodiesel production from *Jatropha* oil with high AV under the given conditions in Section 2.3. In Table 1, biodiesel yield grew remarkably from 46.4% to 84.6% with increased Na_2SiO_3 weight from 0.5 to 8.0 g during catalyst preparation at calcination temperature of 400 °C, since basic groups helped to catalyze the transesterification of triglycerides. Biodiesel yield declined from 46.4% to 15.0% along with calcination temperature rise from 400 to 600 °C (with 0.5 g Na_2SiO_3 added) because of a decrease in acid content of

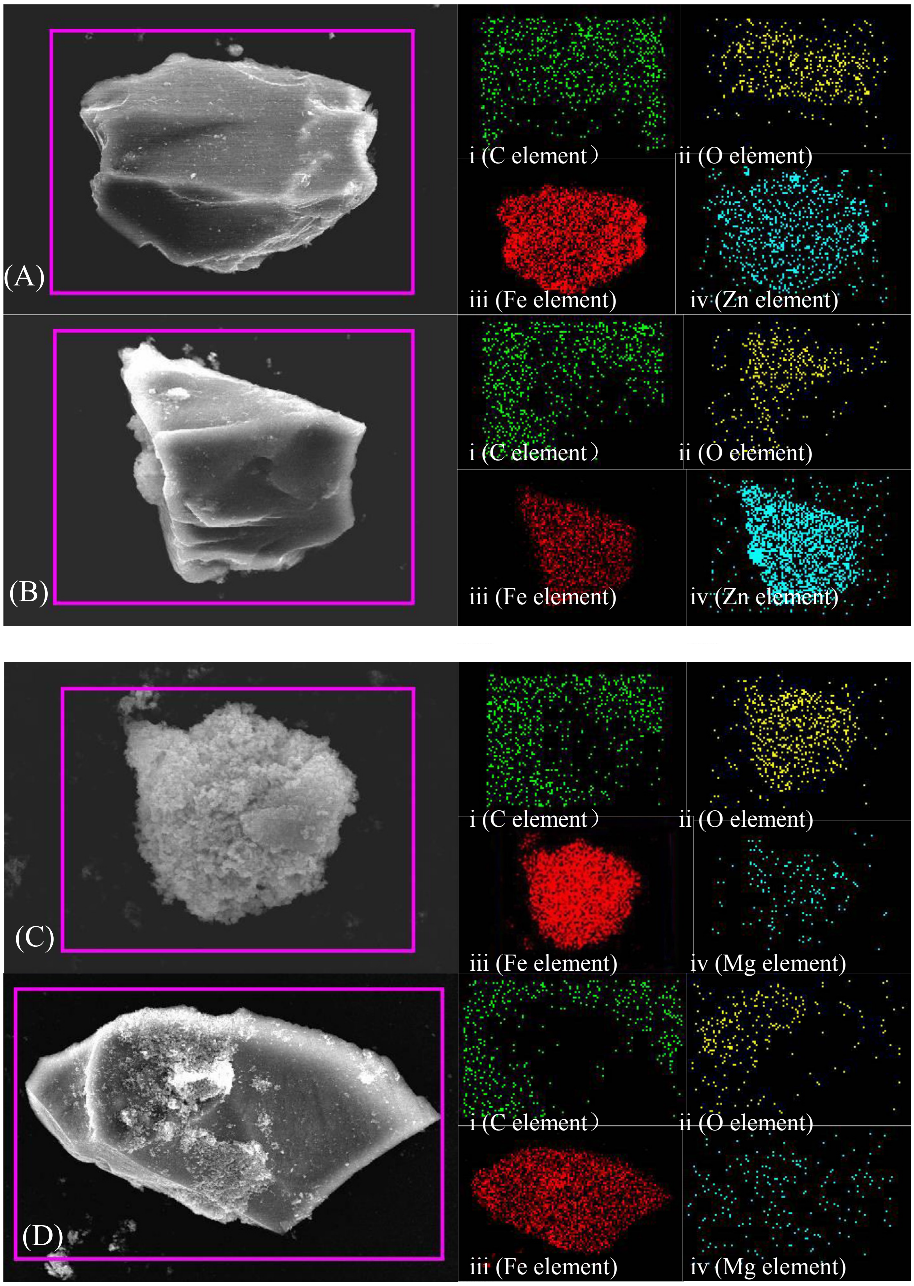

Fig. 3. EDX maps of (A) fresh Zn_8@Fe-C_{400}, (B) recovered Zn_8@Fe-C_{400} catalyst after 5 cycles, (C) fresh Mg_8@Fe-C_{600}, and (D) recovered Mg_8@Fe-C_{600} catalyst after 5 cycles.

catalysts due to more -COOFe reduced to Fe_3O_4. While biodiesel yield increased from 84.6% to 99.4% with calcination temperature increasing from 400 to 600 °C (with 8.0 g Na_2SiO_3 added, Table 1) due to the catalytic activity mainly coming from the basic groups. Obviously, high calcination temperature benefited biodiesel production but resulted in observable saponification. It was found that biodiesel was saponified into solid after stored for several days since the by-product water from the esterification reaction would hydrolyze FAMEs to FFAs that would react with dissolved Na^+ to form sodium aliphatate (saponification). So, Na_n@Fe-C_T catalysts were not suitable for catalyzing high AV oil.

3.1.2. Production of biodiesel over magnetic Al-based amphoteric catalysts

Al-, Mg- and Zn-based amphoteric catalysts (no saponification during reactions and storage was found) were synthesized for biodiesel production. According to Table 2, Al-based amphoteric catalysts had much weaker activity from their weak acid and base content, with biodiesel yield of 15.2–64.9%. The magnetism of Al_8@Fe-C_T amphoteric catalysts was also weak, and hard to be recovered after reactions for recycles. So they were not selected.

3.1.3. Production of biodiesel over magnetic Mg-based amphoteric catalysts

Mg_n@Fe-C_T catalysts showed excellent catalytic capacity than Al_n@Fe-C_T, with the highest biodiesel yield of 99.0% for Mg_8@Fe-C_{600}. Similar to Na-base amphoteric catalysts, when 2.0 or 4.0 g MgO was added, catalyst activity decreased with an increase in calcination temperature (Table 3). However, high calcination temperature benefited biodiesel production over Mg_8@Fe-C_T catalysts (with 8.0 g MgO). It was possibly attributed to the concerted effect of acidic and basic sites over catalyst surface. Appropriate higher calcination temperature improved the activity of solid base mainly for transesterification reaction [32], which was more noticeable for Mg_8@Fe-C_T catalysts. Obviously, Mg_8@

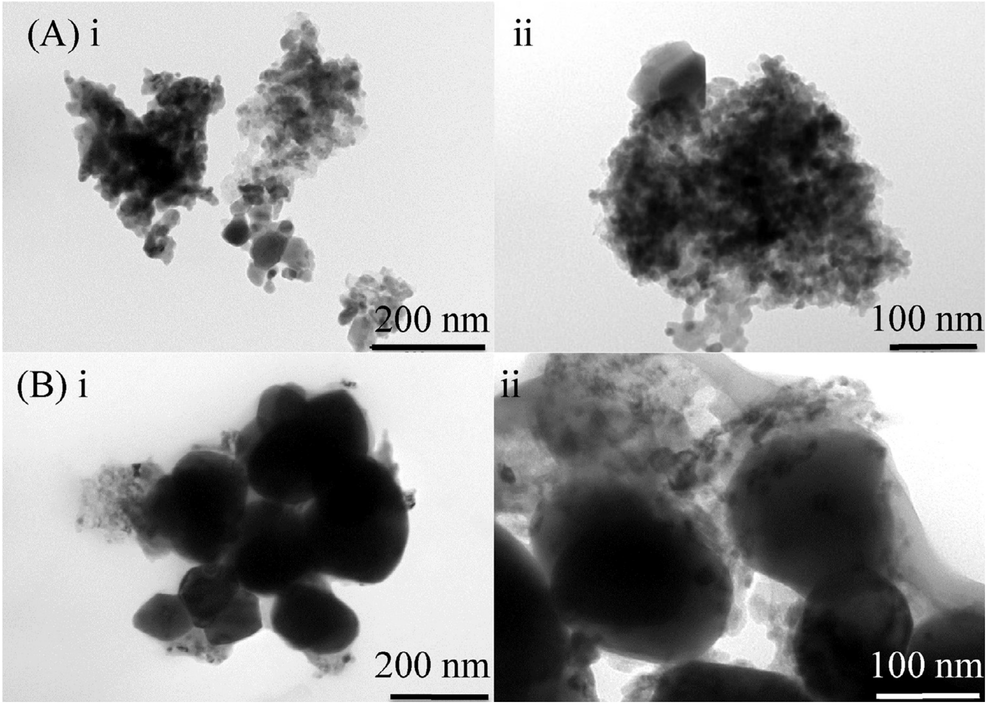

Fig. 4. TEM images of (A) fresh $Zn_8@Fe\text{-}C_{400}$ and (B) $Mg_8@Fe\text{-}C_{600}$ catalysts.

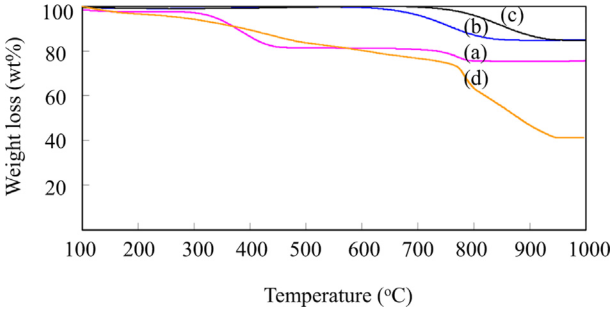

Fig. 5. Thermal stability of (a) fresh $Zn_8@Fe\text{-}C_{400}$,(b) $Zn_8@Fe\text{-}C_{500}$,(c) $Zn_8@Fe\text{-}C_{600}$ catalysts and (d) recovered $Zn_8@Fe\text{-}C_{400}$ after 5 cycle.

$Fe\text{-}C_{600}$ catalyst may be suitable for one-step biodiesel production, so, stability test was very necessary.

3.1.4. $Mg_8@Fe\text{-}C_{600}$ catalyst recycles

In order to understand the reusability of $Mg_8@Fe\text{-}C_{600}$ catalyst, it was tested at the above reaction conditions for 5 cycles. Biodiesel yield was 99.0 ± 0.8%, 88.5 ± 0.3%, 39.4 ± 2.1%, 33.6 ± 0.1% and 28.8 ± 0.2% for 5 cycles with > 80% recovery rate, separately. Although the $Mg_8@Fe\text{-}C_{600}$ catalyst showed very excellent catalytic ability in the first cycle, its stability was poor because Mg after calcination was easy to be impregnated [11]. Hence, it was not suitable for industrial application.

3.1.5. Production of biodiesel over magnetic Zn-based amphoteric catalysts

The activity of $Zn_n@Fe\text{-}C_T$ catalysts was obviously improved with the increase of ZnO amount and the decrease of calcination temperature (Table 4). The highest biodiesel yield of 100.0% was achieved over $Zn_8@Fe\text{-}C_{400}$ catalyst, which was higher than any other catalysts we tested in this study. So, catalyst $Zn_8@Fe\text{-}C_{400}$ was selected to see its reusability.

3.1.6. $Zn_8@Fe\text{-}C_{400}$ catalyst recycles

$Zn_8@Fe\text{-}C_{400}$ catalyst could be successfully recovered using a magnet after biodiesel production, while the catalytic activity of recovered catalyst was tested in biodiesel production under the same conditions. Biodiesel yield was 100.0 ± 0.0%, 99.2 ± 1.1%,

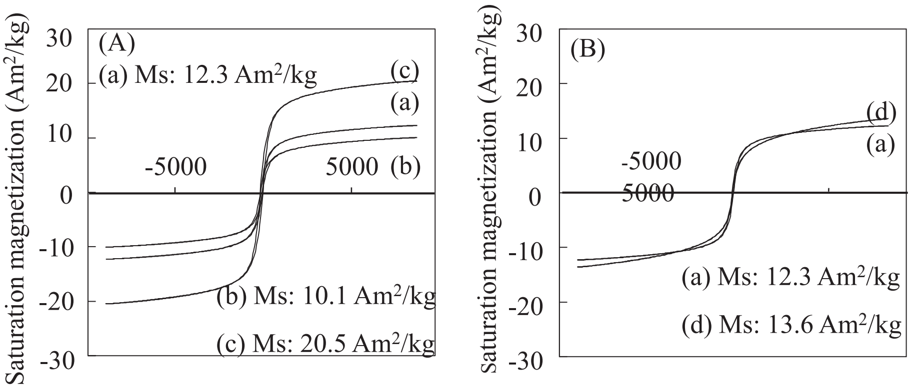

Fig. 6. Hysteresis loops of (A) fresh $Zn_8@Fe\text{-}C_T$ [(a) $Zn_8@Fe\text{-}C_{400}$, (b) $Zn_8@Fe\text{-}C_{500}$ and (c) $Zn_8@Fe\text{-}C_{600}$ catalysts], and (B) fresh and recovered $Zn_8@Fe\text{-}C_{400}$ catalyst after 5 cycles [(a) fresh and (b) recovered catalyst].

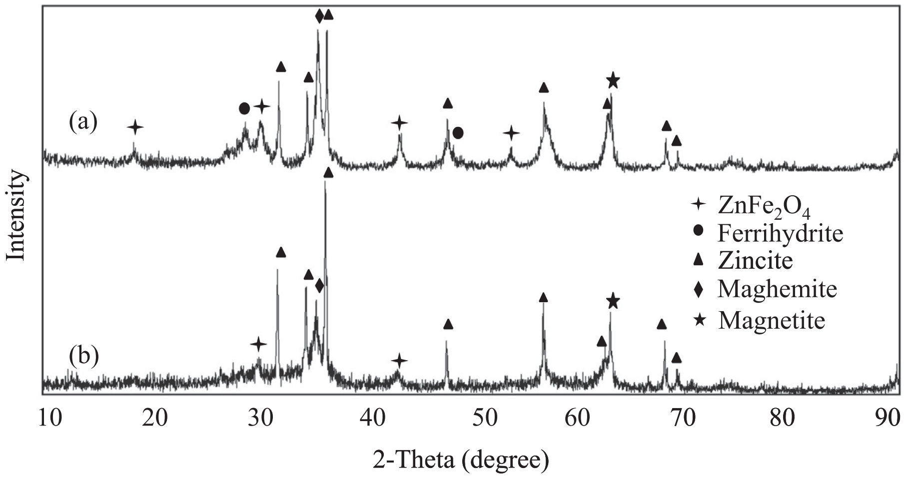

Fig. 7. XRD patterns of (a) Zn_8@Fe-C_{400} and (b) recovered Zn_8@Fe-C_{400} catalyst after 5 cycles.

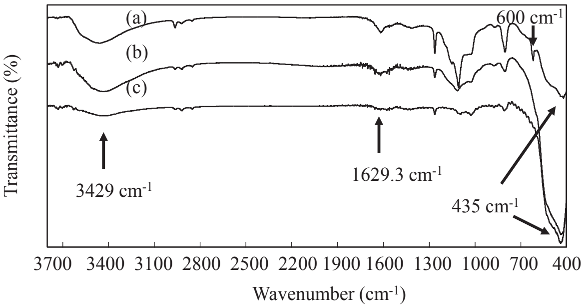

Fig. 8. FT-IR spectra of (a) fresh Zn_8@Fe-C_{400}, (b) Zn_8@Fe-C_{500} and (c) Zn_8@Fe-C_{600} catalysts.

Table 5
Temperature programmed desorption (TPD) analysis of fresh and recovered catalysts.

Catalysts	Acidity (mmol/g)	Basicity (mmol/g)
Zn_8@Fe-C_{400} Fresh	2.74	3.16
Recovered catalyst after 5 cycles[a]	2.59	0.74
Zn_8@Fe-C_{500} Fresh	1.65	0.84
Zn_8@Fe-C_{600} Fresh	1.14	0.48
Mg_8@Fe-C_{400} Fresh	0.99	1.93
Mg_8@Fe-C_{500} Fresh	2.36	2.68
Mg_8@Fe-C_{600} Fresh	3.90	0.60
Recovered catalyst after 5 cycles[a]	1.15	0.34
Na_8@Fe-C_{600} Fresh	1.29	0.80
Al_8@Fe-C_{600} Fresh	0.93	0.18

[a] Reaction conditions: 160 °C, 4.5 MPa, 4 h, catalyst dosage of 7 wt%, methanol/oil molar ratio of 40/1 with 4.3 g *Jatropha* oil (AV of 6.3 mg KOH/g), magnetic stirring of 750 rpm and initial N_2 pressure of 2 MPa (recovered catalyst was washed with ethanol for next runs).

95.6 ± 0.0%, 95.3 ± 0.1% and 86.0 ± 0.5% for five cycles with > 80% recovery rate, respectively.

Reactions were conducted with more samples: *Jatropha* oil (8.6 g), dehydrated methanol (12.8 g) and catalyst (0.6 g) to find out the effect of dead space (9.5 mL volume) in the autoclave on biodiesel yield. Biodiesel yield was 100.0 ± 0.0%, 97.3 ± 0.8%, 94.2 ± 0.4%, 94.2 ± 0.2%, 94.6 ± 0.7%, 94.8 ± 1.0%, 94.4 ± 0.6%, 94.7 ± 1.3%, 95.8 ± 1.2% and 94.3 ± 0.8% for 10 cycles which suggested that the main reason for biodiesel yield decreasing was the effective liquid methanol reduction (less methanol was used to match the ratio to oil or decreased recycled catalyst during cycles) that evaporated to the dead space of the autoclave during reactions. After 3 cycles, biodiesel yield declined from 100.0% to 94.2% and kept stable, the reasons for the yield decline slightly were: (i) loss of basic sites; and (ii) glycerol remained on the surface of the catalyst. The result seemed to be acceptable as compared to previous literature [33]. So, Zn_8@Fe-C_{400} catalyst was regarded as the most proper catalyst for the one-step synthesis of biodiesel from high AV *Jatropha* oil, and was characterized using many technologies next.

3.1.7. Production of biodiesel over ZnO catalyst

For comparison, pure ZnO was also calcined at 400 °C for 2 h, and used to catalyze *Jatropha* oil under similar conditions. Pure ZnO (0.13 g) was added in the reaction to ensure the same usage of ZnO compared to the reaction over Zn_8@Fe-C_{400}. The result demonstrated that Zn_8@Fe-C_{400} provided better biodiesel yield (100.0%) than calcined basic ZnO (88.7 ± 0.5%), which meant that acidic catalysis from both activated ZnO and -COOFe made significant contribution to the one-step esterification and transesterification of high AV oils. It is interesting that *Jatropha* biodiesel catalyzed by ZnO after stored for half year at room temperature was saponified (Fig. 1B). But, no saponification phenomenon was observed for *Jatropha* biodiesel catalyzed by Zn_8@Fe-C_{400} (Fig. 1A), indicating that Zn_8@Fe-C_{400} was very stable.

3.1.8. Production of biodiesel from different AV oils over Zn_8@Fe-C_{400} catalyst

Crude *Jatropha* oils with AV of 6.3, 12.8 and 17.3 mg KOH/g were selected for one-step production of biodiesel to test catalyst tolerance capacity to FFAs contents. *Jatropha* biodiesel yields of 100.0 ± 0.0%, 98.5 ± 0.3% and 98.3 ± 0.9% were achieved at AV of 6.3, 12.8 and 17.3 mg KOH/g, respectively. The introduction of appropriate acid and base contents could make catalyst resist certain amount of FFAs in raw oils.

3.2. Catalysts characterization

By comparing the TPD results, it was found that the acid and base contents of catalysts mainly decided their catalytic activities. In Table 5, acidity and basicity of Zn_8@Fe-C_T catalysts declined from 2.74 to 1.14 mmol/g, and 3.16 to 0.48 mmol/g, respectively, as calcination temperature increased from 400 to 600 °C. Their corresponding activities decreased with biodiesel yields reduced from 100.0% to 89.1%. The basicity of Zn_8@Fe-C_T catalysts was mainly dependent on the basic ZnO, $ZnFe_2O_4$ and other metal oxides, while their acidity was regarded as the result of -COOFe structure produced by the chelation of Fe^{3+} ion with CMC. The increase of calcination temperature from 400 to 600 °C possibly resulted in the decarboxylation of -COOFe and the adverse

Table 6
BET surface area, pore volume and pore size analysis of fresh and recovered catalysts.

Catalysts	BET surface area (m^2/g)	Pore volume (cm^3/g)	Pore size (nm)
Zn_8@Fe-C_{400} Fresh	37.38	0.03	7.45
Recovered catalyst after 5 cycles[a]	5.60	0.03	12.86
Zn_8@Fe-C_{500} Fresh	17.19	0.06	20.57
Zn_8@Fe-C_{600} Fresh	28.14	0.11	24.88
Mg_8@Fe-C_{400} Fresh	29.83	0.14	1.31
Mg_8@Fe-C_{500} Fresh	23.82	0.18	2.85
Mg_8@Fe-C_{600} Fresh	34.57	0.08	1.60
Recovered catalyst after 5 cycles[a]	6.64	0.05	27.03
Al_8@Fe-C_{600} Fresh	121.84	0.35	7.39
Na_8@Fe-C_{600} Fresh	111.48	0.10	9.75

[a] Reaction conditions: 160 °C, 4.5 MPa, 4 h, catalyst dosage of 7 wt%, methanol/oil molar ratio of 40/1 with 4.3 g *Jatropha* oil (AV of 6.3 mg KOH/g), magnetic stirring of 750 rpm and initial N_2 pressure of 2 MPa (recovered catalyst was washed with ethanol for next runs).

Table 7
The crystalline sizes of fresh Zn_8@Fe-C_{400} and recovered Zn_8@Fe-C_{400} after 5 cycles calculated by Scherer equation from XRD analysis.

Crystal phases	Diffraction angles 2Theta (°)[a]	Average particle size (nm)
Zn_8@Fe-$C_{400}$$ZnFe_2O_4$	43.4 (18.5, 30.3, 53.8)	10.7
Ferrihydrite	28.7 (48.6)	2.5
Zincite	32.0 (34.6, 36.4, 47.7, 56.8,62.7, 68.1, 69.2)	45.4
Maghemite	35.7	45.9
Magnetite	63.1	14.0
Recovered Zn_8@Fe-C_{400} after 5 cycles$ZnFe_2O_4$	43.1 (30.0)	10.0
Ferrihydrite	–	–
Zincite	31.8 (34.5, 36.3, 47.6, 56.7, 62.4, 68.1, 69.2)	40.9
Maghemite	35.4	41.9
Magnetite	63.0	17.2

[a] Data not in parenthesis were used for the calculation of crystalline sizes.

Table 8
Elemental compositions of Zn_8@Fe-C_T and recovered Zn_8@Fe-C_{400} catalysts analyzed by EDX (spot scanning), ICP and element analysis.

Catalysts	C (wt%)	O (wt%)	Zn (wt%)	Fe (wt%)
Zn_8@Fe-C_{400}, fresh	33.5 18.9[b]	24.5	13.0 33.7[a]	27.1 24.1[a]
Zn_8@Fe-C_{400}, after 5 cycles	44.5 21.6[b]	25.8	9.2 22.9[a]	19.5 23.4[a]
Zn_8@Fe-C_{500}, fresh	22.9	14.6	21.9 35.5[a]	38.3 14.7[a]
Zn_8@Fe-C_{600}, fresh	28.9	17.6	37.3 32.3[a]	14.2 24.0[a]

[a] Analyzed by ICP.

[b] Analyzed by elemental analysis.

variation of the crystalline phases of alkaline oxides. For Mg_8@Fe-C_T catalysts, high acid content might resist FFAs on basic sites, thus Mg_8@Fe-C_{600} (acidity of 3.90 mmol/g) achieved higher yield of 99.0% than Mg_8@Fe-$C_{400/500}$ (yields of 90.6 and 96.3%) with acidity of 0.99 and 2.36 mmol/g, separately. However, the acid and base contents of Al_8@Fe-C_{600} catalyst were 0.93 mmol/g and 0.18 mmol/g (with only 64.9% biodiesel yield). The reason for the high yield of 99.4% obtained with Na_8@Fe-C_{600} catalyst was Na in sodium silicate was slightly soluble in methanol [34]. In summary, the stability of acidic groups was very important for the conversion of FFAs and helped to resist FFAs on basic groups. So, the yields of biodiesel by Zn_8@Fe-C_{400} still kept about 94.6% after 5 cycles due to its stable acid sites (acid content of 2.59 mmol/g after 5 cycles). But, catalytic activity of Mg_8@Fe-C_{600} dropped rapidly.

The rise in calcination temperature also changed the physical surface of catalysts (Table 6). The BET surface area of Zn_8@Fe-C_T catalysts decreased to 17.19 from 37.38 m^2/g as calcination temperature increased from 400 to 500 °C and slightly increased further to 28.14 m^2/g at 600 °C. Similar trend appeared for Mg_8@Fe-C_T catalysts with BET surface area of 29.83, 23.82 and 34.57 m^2/g at 400–600 °C, respectively. Al_8@Fe-C_{600} and Na_8@Fe-C_{600} had larger BET surface areas of 121.84 and 111.48 m^2/g, respectively, but poorer activity. The results suggested there was no obvious correlation between BET surface area and activity. Due to the sizes of FFAs and methanol being less than 4 nm [35], the pore sizes of Zn_8@Fe-C_T catalysts (7.45–24.88 nm) were more suitable for FFAs and methanol to enter into the internal channels of catalyst for reactions than Mg_8@Fe-C_T catalyst (1.31–2.85 nm). After 5 cycles, for Zn_8@Fe-C_{400} and Mg_8@Fe-$C_{600,}$ their BET surface areas declined but their pore sizes increased because the flowing of oils and methanol entered during the reactions expanded the pores, and the coverage of glycerol decreased BET surface area. The pore volume of different catalysts changed little (Table 6).

SEM images of fresh and recovered Zn_8@Fe-C_{400} nanoparticles were shown in Fig. 2A-B. The surface of fresh Zn_8@Fe-C_{400} nanoparticle was rough with many holes (Fig. 2A). After 5 cycles, its pores over catalyst surface were mostly covered (Fig. 2B) which was consistent with the results from BET surface area. Mg_8@Fe-C_{600} catalyst had many little spherical particles (Fig. 2C), and there was little change in the surface morphology after 5 cycles (Fig. 2D).

Fig. 3A and B displayed EDX maps of fresh and recovered Zn_8@Fe-C_{400} nanoparticles (The carbon distribution detected was inaccurate because samples was fixed by carbon tape). Comparing the maps in Fig. 3A (iii-iv) and B (iii-iv), after 5 cycles for Zn_8@Fe-C_{400}, Fe content declined, while Zn content increased because -COOFe was slightly leached and zinc oxide inside was exposed. EDX maps of fresh and recovered Mg_8@Fe-C_{600} were showed in Fig. 3C and D. After 5 cycles, C, O and Fe contents obviously decreased, which suggested great loss of -COOFe (its acid content decreased from 3.90 to 1.15 mmol/g).

TEM images of fresh Zn_8@Fe-C_{400} and Mg_8@Fe-C_{600} catalysts (Fig. 4) demonstrated that Zn_8@Fe-C_{400} particle was composed of irregularly shaped carbon shell with metal oxides (Fig. 4A i-ii), while Mg_8@Fe-C_{600} was composed of spherical particles with size of 100–200 nm (Fig. 4B i-ii).

TG curves in Fig. 5 showed that the thermal stability of solid catalysts was enhanced with calcination temperature. Zn_8@Fe-C_{400} nanoparticles mainly decomposed at 300–400 °C (Fig. 5a), with the weight loss of 16.3 wt%. The thermal stability of Zn_8@Fe-$C_{500/600}$ particles was better than Zn_8@Fe-C_{400} due to their higher calcination temperature (Fig. 5b-c). The recovered Zn_8@Fe-C_{400} nanoparticles after 5 cycles lost weight of 21.2% at 300–400 °C and weight of 32.6% at 750–950 °C because the residue glycerol on its surface underwent volatilization and carbonization (Fig. 5d).

The hysteresis loops in Fig. 6 A showed that all three Zn_8@Fe-$C_{400/500/600}$ catalysts had considerable magnetism of 10.1–20.5 Am^2/kg. After 5 cycles, the magnetism of Zn_8@Fe-C_{400} slightly grew from 12.3 to 13.6 Am^2/kg due to the loss of non-functional carbon on its surface (Fig. 6B).

The XRD patterns of fresh and recovered Zn_8@Fe-C_{400} nanoparticles were shown in Fig. 7. According to the cards from Joint Committee on Powder Diffraction Standards (JCPDS: 74–0748, 16–0818), Zn_8@Fe-C_{400} showed well-crystallized structures of $ZnFe_2O_{4,}$ ferrihydrite, zincite, maghemite and magnetite after chelation and calcination, while maghemite and magnetite were formed through the reduction of -COOFe to magnetic Fe_3O_4 during calcination. The temperature of ≥400 °C was necessary, since reduction reaction did not happend at low temperatures [27]. Based on Scherer equation [29], the crystalline sizes of $ZnFe_2O_4$, ferrihydrite, zincite, maghemite and magnetite were 10.7, 2.5, 45.4, 45.9 and 14.0 nm, respectively (Table 7). The recovered Zn_8@Fe-C_{400} only had crystallized structures of $ZnFe_2O_4$, zincite, maghemite and magnetite (Fig. 7b) with crystalline sizes of 10.0, 40.9, 41.9 and 17.2 nm. The crystal diffraction peak intensity of zincite increased, but the intensity for $ZnFe_2O_4$ and maghemite decreased due to $ZnFe_2O_4$ and maghemite over catalyst surface being leached and zincite inside being exposed after reactions. There was no ferrihydrite crystallized structure in the recovered Zn_8@Fe-C_{400} catalyst (EDX maps in the recovered Zn_8@Fe-C_{400} also suggested the loss of Fe).

The FT-IR spectra of Zn_8@Fe-$C_{400/500}$ catalysts (Fig. 8a-b) exhibited obvious absorptions for -OH stretching at 3429 and symmetric stretching of COO^- at 1629 cm^{-1} [25,36], which were both remarkably weakened for Zn_8@Fe-C_{600} catalyst calcined at 600 °C (Fig. 8c). Zn-O stretching was detected at 435 cm^{-1} for all three Zn_8@Fe-C_T catalysts [37,38], while the characteristic band of Fe-O-Fe stretching at around 600 cm^{-1} for Fe_3O_4 was only observed on Zn_8@Fe-C_{400} [39]. However, Zn_8@Fe-C_{500} and Zn_8@Fe-C_{600} catalysts also had certain magnetism (Fig. 6) that may come from magnetic Fe particles.

Elemental compositions of Zn_8@Fe-C_T catalysts were analyzed by EDX (spot scanning), ICP and element analysis, and the results were listed in Table 8. Calcination temperature greatly influenced the migration of metal oxides between bulk catalyst and its surface. For Zn_8@Fe-C_T catalysts, Fe contents in bulk catalyst first declined from 24.1% to 14.7%, and then increased to 24.0% with the rise of calcination temperature from 400 to 600 °C, while Zn contents altered a little (32.3–35.5%). High calcination temperature favored the enrichment of Zn on catalyst surface, with its content increased from 13.0% to 37.3% at 400 and 600 °C, while the surface concentration of Fe first increased from 27.1% at 400 °C to 38.3% at 500 °C, and then decreased to 14.2% at 600 °C. The C and O contents over catalyst surface first decreased and then increased with calcination temperature increasing from 400 to 600 °C, following an inverse relationship with surface Fe. After 5 cycles, the Zn content of recovered Zn_8@Fe-C_{400} in the bulk phase remarkably decreased from 33.7% to 22.9% may be mainly caused by the increase in C content in the bulk phase of 18.9 to 21.6% (element analysis). Comparing the results for Zn contents in the bulk phase (33.7%) with catalyst surface (13.0%), zinc oxides of fresh Zn_8@Fe-C_{400} catalyst mainly enriched inside the catalyst which was consistent with catalyst synthesis scheme. There were more iron oxides (27.1% on the surface *vs.* 24.1% in bulk catalyst) on the surface of the fresh Zn_8@Fe-C_{400} catalyst owing to -COOFe structure formed by chelation on the outside, but less iron oxides (19.5% on the surface *vs.* 23.4% in bulk catalyst) were remained on the surface of the recovered catalyst because ferrihydrite was leached and ($ZnFe_2O_4$ and maghemite) decreased (Fig. 7b). For fresh Zn_8@Fe-C_{400} catalyst, C concentration (33.5% on the surface *vs.* 18.9% in bulk catalyst) on catalyst surface was higher for similar reasons. The adhesion of carbon-rich byproducts caused the increase of C concentration over catalyst surface (from 33.5% to 44.5%) and in bulk catalysts (from 18.9% to 21.6% detected by element analysis) after reactions which led to the surface concentration of Zn dropped to 9.2% (in fact bulk Zn content increased in Fig. 3B-iv). However, the molar ratio of Zn/Fe over catalyst surface was nearly unchanged (0.403 *vs.* 0.410).

4. Conclusions

Biodiesel production from *Jatropha* oils with high AV at low temperature was catalyzed with synthesized magnetic acid-base amphoteric nanoparticles (< 46 nm) via one-pot esterification and transesterification without pretreatment. The results demonstrated that catalyst of Zn_8@Fe-C_{400} presented both high acidity of 2.74 mmol/g, high basicity of 3.16 mmol/g, and strong magnetism of 12.3 Am^2/kg from nanoparticles of $ZnFe_2O_4$, zincite, ferrihydrite, maghemite and magnetite. It can resist free fatty acids to achieve 100.0% *Jatropha* biodiesel yield at AV of 6.3 mg KOH/g and recycle 10 times with biodiesel yield > 94.3% under given conditions: 160 °C, 4.5 MPa, 40/1 methanol/oil molar ratio, 7 wt% catalyst and 4 h reaction time. No macroscopical saponification was observed.

Acknowledgements

The authors wish to acknowledge the financial support from Nanjing Agricultural University (No. 68Q-0603), the Natural Science Foundation of China (No. 31400507, No. 31400518), Natural Science Foundation of Yunnan Province of China (No. 2015FB184) and Youth Innovation Promotion Association CAS (No. 2017440). Thanks are also given to Dr. Fan Zhang and Miss Wen-jing Yang from Xishuangbanna Tropical Botanical Garden.

References

[1] M.M. Hasan, M.M. Rahman, Performance and emission characteristics of biodiesel–diesel blend and environmental and economic impacts of biodiesel production: A review, Renew. Sustain. Energy Rev. 74 (2017) 938–948.
[2] F. Sundus, M.A. Fazal, H.H. Masjuki, Tribology with biodiesel: a study on enhancing biodiesel stability and its fuel properties, Renew. Sustain. Energy Rev. 70 (2017) 399–412.
[3] M.Z. Jacobson, Review of solutions to global warming, air pollution, and energy security, Energy Environ. Sci. 2 (2009) 148–173.
[4] M. Habibullah, H.H. Masjuki, M.A. Kalam, I.M. Rizwanul Fattah, A.M. Ashraful, H.M. Mobarak, Biodiesel production and performance evaluation of coconut, palm and their combined blend with diesel in a single-cylinder diesel engine, Energy Convers. Manage. 87 (2014) 250–257.
[5] M.A. Fazal, A.S.M.A. Haseeb, H.H. Masjuki, Biodiesel feasibility study: an evaluation of material compatibility; performance; emission and engine durability, Renew. Sustain. Energy Rev. 15 (2011) 1314–1324.
[6] S. Rafiei, S. Tangestaninejad, P. Horcajada, M. Moghadam, V. Mirkhani, I. Mohammadpoor-Baltork, R. Kardanpour, F. Zadehahmadi, Efficient biodiesel production using a lipase@ZIF-67 nanobioreactor, Chem. Eng. J. 334 (2018) 1233–1241.
[7] D. Qi, H. Chen, L. Geng, Y. Bian, Experimental studies on the combustion characteristics and performance of a direct injection engine fueled with biodiesel/diesel blends, Energy Convers. Manage. 51 (2010) 2985–2992.
[8] M. Nabi, M. Rahman, S. Akhter, Biodiesel from cotton seed oil and its effect on engine performance and exhaust emissions, Appl. Therm. Eng. 29 (2009) 2265–2270.
[9] Y.D. Long, Z. Fang, T.C. Su, Co-production of biodiesel and hydrogen from rapeseed and *Jatropha* oils with sodium silicate and Ni catalysts, Appl. Energy 113 (2014) 1819–1825.
[10] S.H. Teo, A. Islam, C.H. Ng, N. Mansir, T. Ma, S.Y. Thomas Choong, Y.H. Taufiq-Yap, Methoxy-functionalized mesostructured stable carbon catalysts for effective biodiesel production from non-edible feedstock, Chem. Eng. J. 334 (2018) 1851–1868.
[11] Y.T. Wang, Z. Fang, F. Zhang, B.J. Xue, One-step production of biodiesel from oils with high acid value by activated Mg-Al hydrotalcite nanoparticles, Bioresour. Technol. 193 (2015) 84–89.
[12] H. Pan, H. Zhang, S. Yang, Production of biodiesel via simultaneous esterification and transesterification, in: Z. Fang, R.L. Smith, H. Li (Eds.), Production of Biofuels and Chemicals with Bifunctional Catalysts, Biofuels and Biorefineries, Springer, Singapore, 2017, pp. 307–326.
[13] S.P. Souza, J.E.A. Seabra, Environmental benefits of the integrated production of ethanol and biodiesel, Appl. Energy 102 (2013) 5–12.
[14] J. Sheehan, V. Camobreco, J. Duffield, M. Graboski, H. Shapouri, An overview of biodiesel and petroleum diesel life cycles, 1998, https://www.nrel.gov/docs/legosti/fy98/24772.pdf (accessed 19 April 2018).
[15] A. Demirbaş, Biodegradability of biodiesel and petrodiesel fuels, Energy Sources-A 31 (2008) 169–174.
[16] S.B. Živković, M.V. Veljković, I.B. Banković-Ilić, I.M. Krstić, S.S. Konstantinović, S.B. Ilić, J.M. Avramović, O.S. Stamenković, V.B. Veljković, Technological, technical, economic, environmental, social, human health risk, toxicological and policy considerations of biodiesel production and use, Renew. Sustain. Energy Rev. 79 (2017) 222–247.
[17] M.F. Al-Dawody, S.K. Bhatti, Optimization strategies to reduce the biodiesel Nox effect in diesel engine with experimental verification, Energy Convers. Manage. 68 (2013) 96–104.
[18] A.E. Atabani, A.S. Silitonga, I.A. Badruddin, T.M.I. Mahlia, H.H. Masjuki, S. Mekhilef, A comprehensive review on biodiesel as an alternative energy resource and its characteristics, Renew. Sustain. Energy Rev. 16 (2012) 2070–2093.
[19] R.A. Lee, J.M. Lavoie, From first- to third-generation biofuels: challenges of producing a commodity from a biomass of increasing complexity, Anim. Front. 3 (2013) 6–11.
[20] D.Y.C. Leung, X. Wu, M.K.H. Leung, A review on biodiesel production using catalyzed transesterification, Appl. Energy 87 (2010) 1083–1095.
[21] T.M. Deboni, G.A.M. Hirata, G.G. Shimamoto, M. Tubino, A.J. de Almeida

Meirelles, Deacidification and ethyl biodiesel production from acid soybean oil using a strong anion exchange resin, Chem. Eng. J. 333 (2018) 686–696.

[22] C. Pirez, J.M. Caderon, J.P. Dacquin, A.F. Lee, K. Wilson, Tunable KIT-6 mesoporous sulfonic acid catalysts for fatty acid esterification, ACS Catal. 2 (2012) 1607–1614.

[23] M. Olkiewicz, N.V. Plechkova, M.J. Earle, A. Fabregat, F. Stüber, A. Fortuny, J. Font, C. Bengoa, Biodiesel production from sewage sludge lipids catalysed by Brønsted acidic ionic liquids, Appl. Catal. B-Environ. 181 (2016) 738–746.

[24] M. Huang, J. Luo, Z. Fang, H. Li, Biodiesel production catalyzed by highly acidic carbonaceous catalysts synthesized *via* carbonizing lignin in sub- and super-critical ethanol, Appl. Catal. B-Environ. 190 (2016) 103–114.

[25] P.L. Boey, S. Ganesan, G.P. Maniam, M. Khairuddean, S.E. Lee, A new heterogeneous acid catalyst system for esterification of free fatty acids into methyl esters, Appl. Catal. A-Gen. 433–434 (2012) 12–17.

[26] P.L. Boey, S. Ganesan, G.P. Maniam, M. Khairuddean, Sequential conversion of high free fatty acid oils into biodiesel using a new catalyst system, Energy 46 (2012) 132–139.

[27] Y.T. Wang, Z. Fang, X.X. Yang, Biodiesel production from high acid value oils with a highly active and stable bifunctional magnetic acid, Appl. Energy 204 (2017) 702–714.

[28] H. Fukuda, A. Kondo, H. Noda, Biodiesel fuel production by transesterification of oils, J. Biosci. Bioeng. 92 (2001) 405–416.

[29] A.L. Patterson, The Scherrer formula for X-ray particle size determination, Phys. Rev. 56 (1939) 978–982.

[30] R.H. Perry, D.W. Green, D. Green, Perry's Chemical Engineers' Handbook, Seventh Ed., McGraw-Hill Companies Inc, New York, 1997.

[31] B.J. Xue, J. Luo, F. Zhang, Z. Fang, Biodiesel production from soybean and *Jatropha* oils by magnetic $CaFe_2O_4$-$Ca_2Fe_2O_5$-based catalyst, Energy 68 (2014) 584–591.

[32] C.L. Xu, D.I. Enache, R. Lloyd, D.W. Knight, J.K. Bartley, G.J. Hutchings, MgO catalysed triglyceride transesterification for biodiesel synthesis, Catal. Lett. 138 (2010) 1–7.

[33] H.V. Lee, Y.H. Taufiq-Yap, M.Z. Hussein, R. Yunus, Transesterification of *Jatropha* oil with methanol over Mg-Zn mixed metal oxide catalysts, Energy 49 (2013) 12–18.

[34] F. Zhang, Z. Fang, Y.T. Wang, Biodiesel production directly from oils with high acid value by magnetic Na_2SiO_3@Fe_3O_4/C catalyst and ultrasound, Fuel 150 (2015) 370–377.

[35] L. Geng, G. Yu, Y. Wang, Y.X. Zhu, Ph-SO_3H-modified mesoporous carbon as an efficient catalyst for the esterification of oleic acid, Appl. Catal. A-Gen. 427–428 (2012) 137–144.

[36] J. Wang, X.Y. Lin, X.G. Luo, Y.F. Long, A sorbent of carboxymethyl cellulose loaded with zirconium for the removal of fluoride from aqueous solution, Chem. Eng. J. 252 (2014) 415–422.

[37] J.H. Shen, G. Ma, J.M. Zhang, W.L. Quan, L.C. Li, Facile fabrication of magneticreduced graphene oxide-$ZnFe_2O_4$composites with enhanced adsorption andphotocatalytic activity, Appl. Surf. Sci. 359 (2015) 455–468.

[38] C.L. Wang, X. Tan, J.T. Yan, B. Chai, J.F. Li, S.Z. Chen, Electrospinning direct synthesis of magnetic $ZnFe_2O_4$/ZnO multi-porous nanotubes with enhanced photocatalytic activity, Appl. Surf. Sci. 396 (2017) 780–790.

[39] Zillillah, G.W. Tana, Z. Li, Highly active, stable, and recyclable magnetic nano-size solid acid catalysts: efficient esterification of free fatty acid in grease to produce biodiesel, Green Chem. 14 (2012) 3077–3086.